

Topological melting of the metastable skyrmion lattice in the chiral magnet $\text{Co}_9\text{Zn}_9\text{Mn}_2$

Victor Ukleev,^{1,2,*} Daisuke Morikawa,^{3,4} Kosuke Karube,³ Akiko Kikkawa,³ Kiyoshi Shibata,^{3,5}
Yasujiro Taguchi,³ Yoshinori Tokura,^{3,6,7} Taka-hisa Arima,^{3,8} and Jonathan S. White¹

¹Laboratory for Neutron Scattering and Imaging (LNS),
Paul Scherrer Institute (PSI), CH-5232 Villigen, Switzerland

²Helmholtz-Zentrum Berlin für Materialien und Energie, D-14109 Berlin, Germany

³RIKEN Center for Emergent Matter Science (CEMS), Wako 351-0198, Japan

⁴Institute of Multidisciplinary Research for Advanced Materials (IMRAM), Tohoku University, Sendai 980-8577, Japan

⁵Institute of Industrial Science, The University of Tokyo, Tokyo 153-8505, Japan

⁶Department of Applied Physics, University of Tokyo, Tokyo 113-8656, Japan

⁷Tokyo College, University of Tokyo, Tokyo 113-8656, Japan

⁸Department of Advanced Materials Science, University of Tokyo, Kashiwa 277-8561, Japan

In a β -Mn-type chiral magnet $\text{Co}_9\text{Zn}_9\text{Mn}_2$, we demonstrate that the magnetic field-driven collapse of a room temperature metastable topological skyrmion lattice passes through a regime described by a partial topological charge inversion. Using Lorentz transmission electron microscopy, the magnetization distribution was observed directly as the magnetic field was swept antiparallel to the original skyrmion core magnetization, i.e. negative magnetic fields. Due to the topological stability of skyrmions, a direct transition of the metastable skyrmion lattice to the equilibrium helical state is avoided for increasingly negative fields. Instead, the metastable skyrmion lattice gradually transforms into giant magnetic bubbles separated by 2π domain walls. Eventually these large structures give way to form a near-homogeneously magnetized medium that unexpectedly hosts a low density of isolated skyrmions with inverted core magnetization, and thus a total topological charge of reduced size and opposite sign compared with the initial state. A similar phenomenon has been observed previously in systems hosting ordered lattices of magnetic bubbles stabilized by the dipolar interaction and called “topological melting”. With support from numerical calculations, we argue that the observed regime of partial topological charge inversion has its origin in the topological protection of the starting metastable skyrmion state.

I. INTRODUCTION

A magnetic skyrmion is a topological object with vortex-like swirling spin configuration, which is characterized by an integer termed the topological number:

$$n = \frac{1}{4\pi} \int \mathbf{M} \cdot \left(\frac{\partial \mathbf{M}}{\partial x} \times \frac{\partial \mathbf{M}}{\partial y} \right) dx dy. \quad (1)$$

Here \mathbf{M} is a unit vector describing the direction of a smoothly varying local magnetization. A skyrmion crystal (SkX) is a periodic, usually triangular-coordinated arrangement of skyrmion. It is a non-trivial collective topological magnetic state that is robust against perturbations, such as magnetic fields and thermal agitation, since it cannot be continuously transformed into an alternative state with smoothly varying magnetization which is described by a different topology [1, 2]. Indeed, in real systems the stability of skyrmions is limited due to the violation of the continuous limit at the atomic scale, the presence of defects or edges, and temperature fluctuations. In the past decade, several kinds of magnets have been found to host skyrmion ($n = -1$) [3–8], bi-skyrmion ($n = -2$) [9–12], or anti-skyrmion

($n = +1$) [13] textures. Note that since n reverses its sign under time reversal, the above topological numbers are given for a common polarity of the core [14].

Skyrmions can be manipulated by ultra-low density electric currents, making them promising for spintronics applications [2, 15]. In bulk materials, skyrmions have been studied extensively in chiral cubic magnets such as the $B20$ -type compounds [3–5, 16–18] and β -Mn-type Co-Zn-Mn alloys [6, 19–24]. In these compounds, due to the interplay between the exchange interaction and the Dzyaloshinskii-Moriya interaction (DMI), a helical magnetic ordering becomes stable upon cooling below a critical temperature (T_c) in zero field. By the application of a moderate magnetic field just below T_c , the helical structure transforms into the ordered triangular SkX. At the mean-field level [25], both the characteristic helical pitch λ and skyrmion size are determined by the ratio of the exchange stiffness A_{ex} to the Dzyaloshinskii constant D , according to $\lambda = 4\pi A_{ex}/D$.

In contrast, periodic lattices of magnetic bubbles can be stabilized in thin films of centrosymmetric magnets with easy axis anisotropy [27–29]. The in-plane rotation sense of the magnetization around the bubble core is non-degenerate, thus leading to a cancellation of the total magnetic chirality and therefore the topological charge of the bubble lattice [30, 31]. This is different

* victor.ukleev@psi.ch

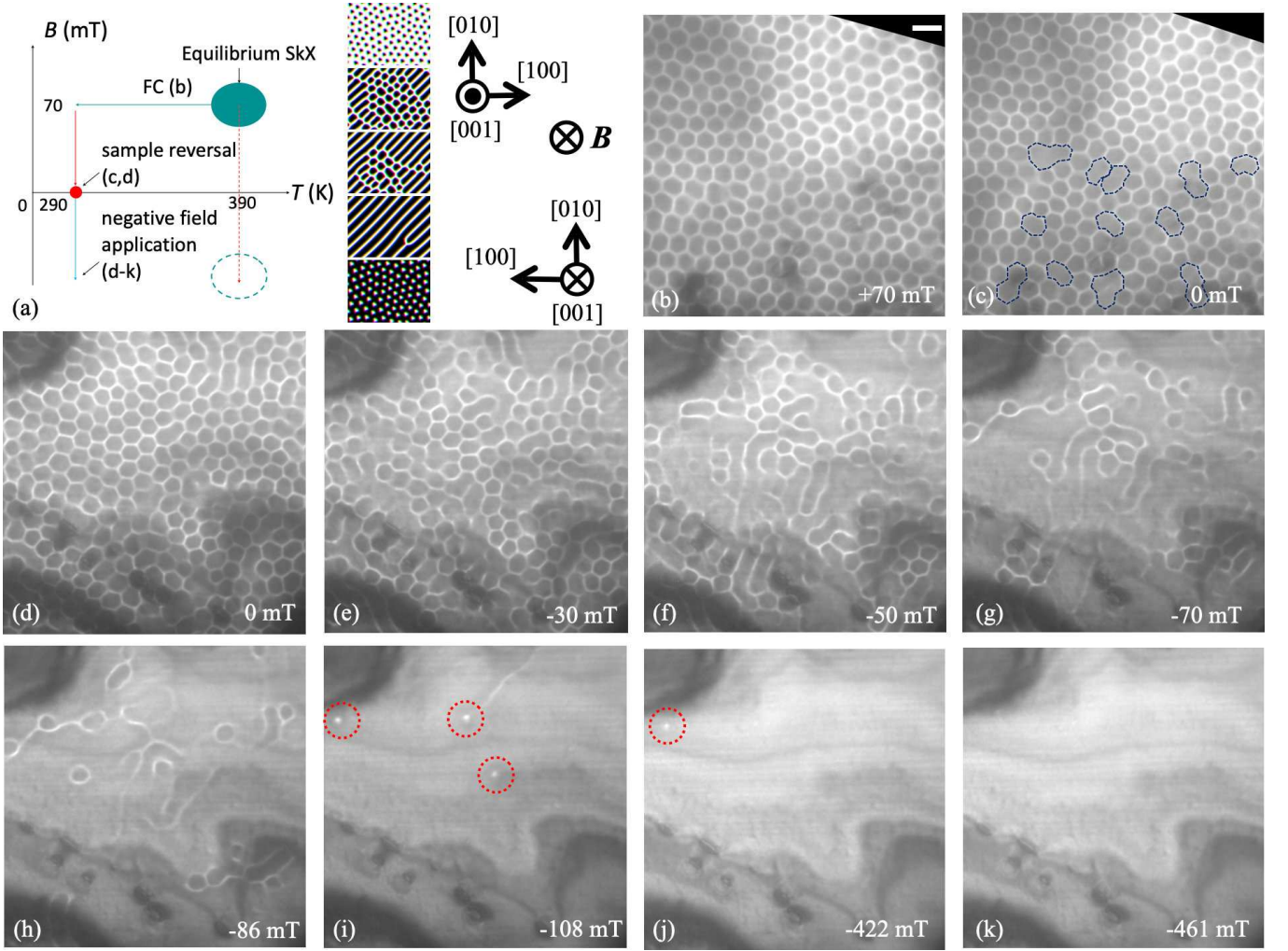


FIG. 1. (a) Schematic illustration of the measurement process. On the left side of (a), the labels (b-k) describes the points in the schematic phase diagram where the data shown in the corresponding panels were collected. The middle of (a) show a sketch the field-driven magnetic texture reversal of the equilibrium phases just below T_c [26]. The right side of (a) shows the crystallographic orientation of the thin plate with respect to the applied magnetic field before (top panel) and after sample reversal (bottom panel), respectively (see text for details). (b) Over-focused LTEM images on the (001) plane after the FC process from 390 K to 290 K at 70 mT. The crystal orientation and field direction are indicated in (a). (c) LTEM image of the zero-field SkX. Merged skyrmions are indicated by dashed blue lines. (d – k) Under-focused LTEM images of the sample after reversal. Each panel corresponds to the evolution of the magnetic structure upon application of the magnetic field in the negative direction compared to the original state. Skyrmions with reversed cores are indicated in panels (i – j) by dashed red circles. The scale bar shown in (b) is 200 nm.

from skyrmion systems where the magnetic chirality is determined by the sign of DMI which itself is determined by the handedness either the chiral crystal, [32, 33] or the interfacial symmetry breaking in magnetic multilayer systems. The research of magnetic bubble domains has existed since the second half of the 20th century, leading to many intriguing observations and theoretical developments. In particular, a coherent inversion of the bubble lattice in garnet films has been experimentally observed upon reversing the direction of applied magnetic field and called "topological switching" [28, 34–36]. An alternative mechanism of magnetic bubble lattice collapse via

the formation of cellular domains was called "topological melting" [37, 38]. Both scenarios were successfully reproduced numerically via a fine-tuning of short-range ferromagnetic and long-range antiferromagnetic dipolar interactions [39]. According to a more recent theory that includes the DMI, it is suggested that the magnetization switching processes of both magnetic skyrmions in chiral magnets, [14] and films with the interfacial DMI and perpendicular magnetic anisotropy (PMA), [40] are accompanied by the nucleation of skyrmion-antiskyrmion or meron-antimeron pairs during the reversal process [41]. It is also proposed that for increasingly negative

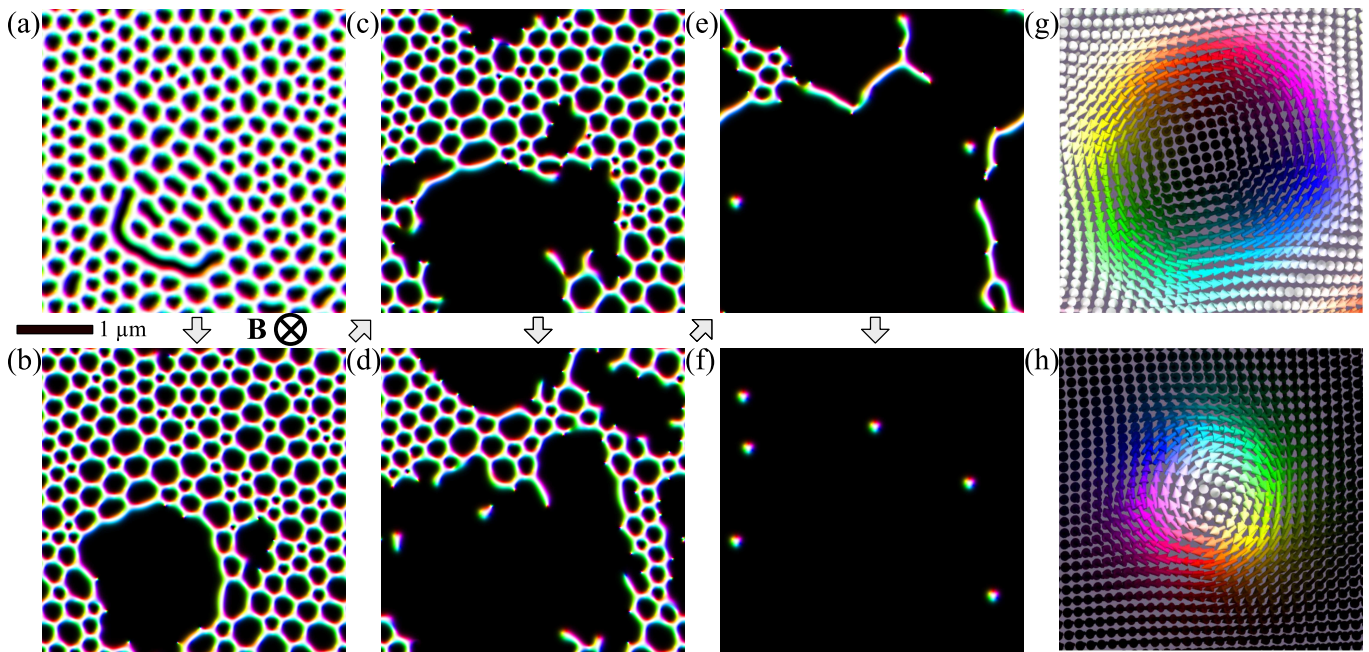


FIG. 2. Micromagnetic simulations of the SkX in a $\text{Co}_9\text{Zn}_9\text{Mn}_2$ thin plate in (a) zero and negative magnetic fields (b) $B = -280$ mT, (c) $B = -285$ mT, (d) $B = -290$ mT, (e) $B = -295$ mT, and (f) $B = -310$ mT. Detailed illustrations of the magnetization distributions for the original zero-field and inverted skyrmions shown in panels (a–f) are given in panels (g,h), respectively. The in-plane magnetization direction is indicated by the colors shown in panels (g,h).

magnetic fields, a defect-free triangular SkX will undergo a first-order topological phase transition to an inverted skyrmion phase via a regime of transient anti-skyrmions [40]. This scenario is analogous to the "topological switching" phenomena in the bubble lattice. In the presence of defects, the transition becomes smeared so that it appears continuous [40] and thus ascribed as "topological melting".

Recently, the β -Mn-type chiral magnet $\text{Co}_9\text{Zn}_9\text{Mn}_2$, with Curie temperature $T_c = 400$ K, was shown to exhibit a robust metastable SkX state at room temperature after field-cooling (FC) through the equilibrium SkX phase that is stable just below T_c [20]. At room temperature, the practically infinite relaxation time of this metastable state makes this compound very promising for certain applications, and a model system for investigating the topological stability of metastable magnetic skyrmions. Indeed the enhanced stability of the metastable SkX in $\text{Co}_9\text{Zn}_9\text{Mn}_2$ at room temperature allows for the investigation of the field-induced transformations of the skyrmion spin texture with a reduced influence of the thermal fluctuation effect [42]. Here we exploit the robust metastable room-temperature SkX in thin plate samples of $\text{Co}_9\text{Zn}_9\text{Mn}_2$ to address the magnetic field-driven magnetization reversal process experimentally, and investigate the "topological switching" or "topological melting" scenarios.

II. RESULTS AND DISCUSSION

A schematic illustration of both the magnetic phase diagram of $\text{Co}_9\text{Zn}_9\text{Mn}_2$ and the measurement protocol are given in Figure 1a. A sketch of the magnetic texture evolution upon magnetic field reversal just below T_c is shown schematically in the middle of the panel. In this case, the thermal equilibrium SkX transitions to the helical structure through the merging of skyrmions firstly into elongated bands, followed by the coherent nucleation of a hexagonal lattice of the reversed skyrmions. This scenario has been confirmed for a 100 nm-thick plate of FeGe at $T = 240$ K [26]. We note that in the current setup, it was not possible to test the same protocol of SkX reversal in the thermal equilibrium SkX phase of $\text{Co}_9\text{Zn}_9\text{Mn}_2$ at $T \sim 370$ K, [19] since the magnetic field direction provided by the objective lens of the TEM could not be reversed. Therefore, the metastability and significantly long lifetime of the room-temperature and zero-field skyrmions in $\text{Co}_9\text{Zn}_9\text{Mn}_2$ was of a critical importance.

The main experimental finding of the present work is shown in Figures 1b–k. Initially, a triangular-lattice SkX state with a lattice constant $a_{Sk} \approx 150$ nm is formed as the equilibrium state at approximately 370 K and 70 mT [20]. Upon FC the sample in $B = 70$ mT from the equilibrium SkX phase to room temperature (290 K), a robust metastable SkX is achieved which serves as our starting state (Figure 1b). As discussed previously for a bulk

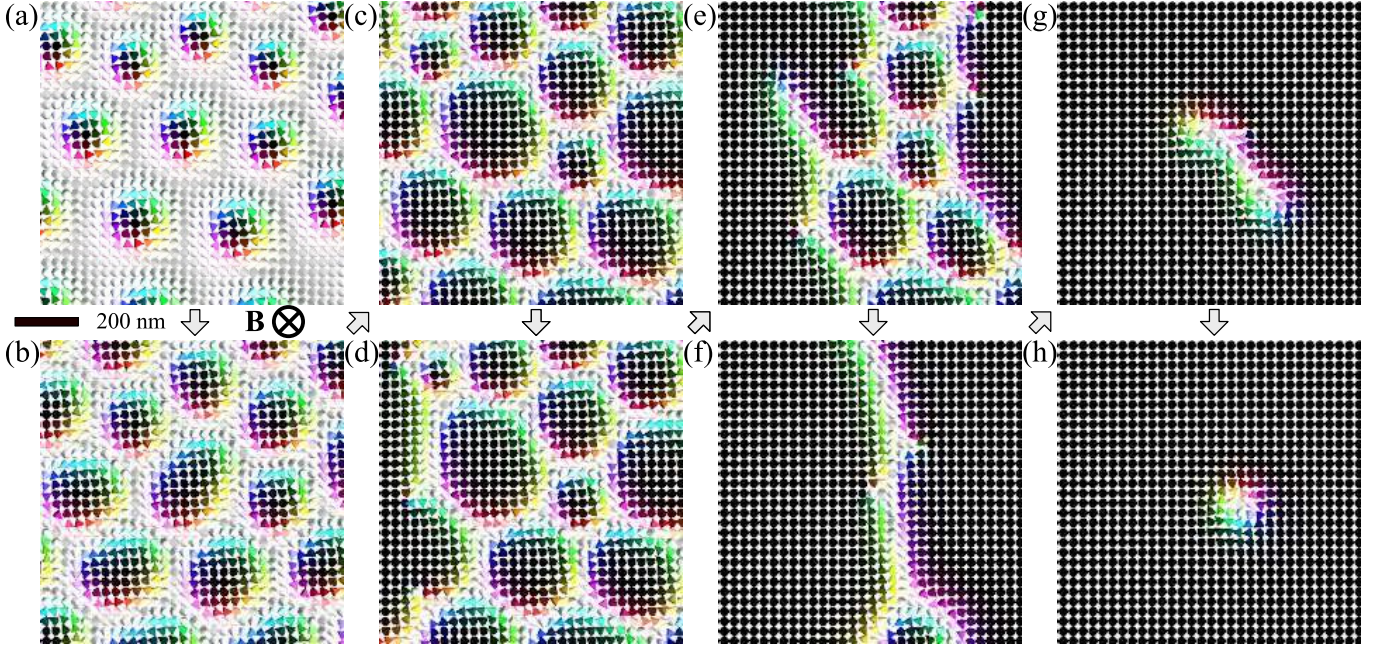


FIG. 3. Magnified view of the magnetization patterns obtained from micromagnetic simulations in (a) positive field $B = +225$ mT, (b) zero field, and negative fields (c) $B = -275$ mT, (d) $B = -285$ mT, (e) $B = -290$ mT, (f) $B = -295$ mT, (g) $B = -300$ mT, and (h) $B = -310$ mT.

sample of $\text{Co}_9\text{Zn}_9\text{Mn}_2$ [20], the metastable SkX at 290 K persists even after the magnetic field is reduced to zero. We find however, that already at zero field the expansion of skyrmion cores and the merging of some skyrmions into larger structures indicated by dashed blue lines in Figure 1c. These effects lead to a reduction of the overall topological charge (i.e. number of skyrmions). Notably, no transformation from the SkX to either a helical state [26, 43] or meron-antimeron lattice [44] is observed in weak magnetic fields.

Since the magnetic field direction provided by the objective lens of the TEM cannot be reversed, the investigation of the negative field evolution of the magnetization distribution was done by removing the sample from the TEM at zero field, and turning it upside-down before re-installing it back into the TEM. The defocus distances for the corresponding LTEM images before and after the 180° reversal of the sample were reset from positive ($+288 \mu\text{m}$) to negative ($-288 \mu\text{m}$) values (Figure 1d), and show almost the same magnetic contrast at zero field. Note that after the sample rotation, the applied external magnetic field is in the same direction in the laboratory frame of reference, i.e. parallel to the skyrmion core magnetization of the starting metastable state. Hereafter, we denote the original direction of the field during FC as positive, and the field applied after the sample reversal as negative.

By increasing the magnitude of the field in the negative direction, skyrmions continue to merge with

each other and the total topological charge decreases further (Figure 1e). Upon sweeping the magnetic field from 0 to -50 mT, the merging of skyrmions results in the creation and inflation of large skyrmion bubbles with a size of $5 - 10a_{Sk}$ (Figure 1e). This phenomenon is consistent with a theoretically predicted scenario in which the SkX transforms into highly unstable large hexagonal cells, which eventually elongate into spiral states [45].

On further increment of the negative magnetic field the bubbles expand, and we observe a peculiar web of skyrmions and bubbles connected to each other by 2π domain wall strings (Figure 1g-h). In this configuration, the total topological charge still has the same sign as the original SkX state, though the magnitude is much smaller. Skyrmion core reversal occurs for negative magnetic fields below -100 mT (Figure 1i-j). The inversion of the skyrmion core magnetization is accompanied by the reversal of the rotation sense of the in-plane magnetization, which shows up experimentally by a change in LTEM contrast: skyrmions with core magnetizations aligned antiparallel to the magnetic field appear as white dots (indicated by dashed red circles in Figures 1i-j). Interestingly, the reversed skyrmion core is much smaller than the original one at 0 T, and its profile changes from hexagonal to circular. This can be understood as a field-driven core collapse, similar to a previous observation of the metastable SkX in FeGe under a high positive magnetic field [46]. This core collapse behavior has been predicted generally to take

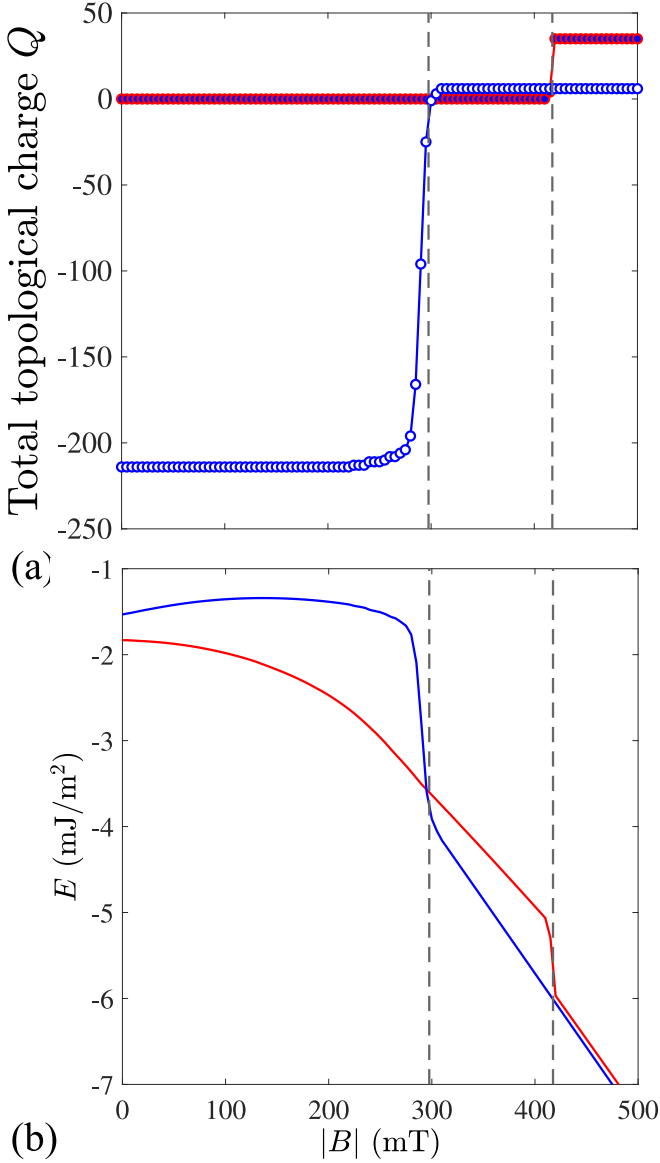


FIG. 4. Plot of (a) the total topological charge Q , and (b) the total energy of the system against external negative field (i.e. a field anti-parallel to the cores of the skyrmions initially stabilised in the case of SkX inversion) derived the micromagnetic simulations. The cases of SkX inversion and SkX nucleation from the helical phase are indicated respectively in each panel by blue and red curves.

place in chiral magnets with uniaxial anisotropy, [1] and is also observed in a skyrmion-hosting monolayer system [47]. Crucially, in the reversed state the total topological charge Q (number of reversed skyrmions) has changed sign, while the magnitude evaluated for the presently studied viewing region of the sample is $\sim 1\%$ of its original value. Finally, all skyrmions are destroyed by a magnetic field of $B = -461$ mT and the sample crosses over to a conical or induced ferromagnetic state (Figure 1k).

An interesting question concerns the detailed magnetic structure of the inverted skyrmions and, especially, the 2π domain walls appearing upon the magnetization reversal. In principle this could be determined by means of a transport-of-intensity equation (TIE) analysis when the timescale of the magnetic dynamics are slower than that of the relevant LTEM measurements. Unfortunately, due to the metastable character of the observed textures, and, consequently, their dynamic behaviour at the timescale of tens of minutes, it was not possible to measure the series of images with different defocus distances required for a TIE analysis. However, this might be possible in future experiments at lower temperatures where the lifetime of metastable states exceeds the time scale of the experiment.

Next we describe how the experimentally observed negative magnetic field-induced collapse of the SkX agrees with the results of Landau-Lifshitz-Gilbert (LLG) simulations. Our calculations were performed using the MuMax³ package [48], and appropriate magnetic parameters for a $\text{Co}_9\text{Zn}_9\text{Mn}_2$ thin plate [49]. The details of the micromagnetic simulation and the simulation code are given in the Supplementary materials. The topological charge on a discrete lattice was quantified using the definition of Berg and Lüscher [50].

To follow the experimental FC protocol, we started the simulation with a random initial magnetization and applied a magnetic field in the positive direction. After 2 ns of relaxation, the magnetic field was removed and the resultant zero-field SkX had a negative field imposed. The magnetization of the system in negative magnetic fields was recorded every 5 mT with a relaxation time of 2 ns between the steps. The results are shown in Figure 2. Although the magnitudes of the magnetic fields in the simulation differ from the experimental values, the process of the skyrmion collapse is qualitatively reproduced. The discrepancy between the measured and simulated negative magnetic field ranges of skyrmion stability can originate from thermal fluctuations, the presence of defect sites, or the role of demagnetization fields in the real experiment.

Consistent with our real-space observations, the simulations show that the collapse process of the SkX starts from elongated (merged) skyrmions that are already present in the sample at zero field (Figures 2a–c). Furthermore, the expansion of skyrmion cores and their merging behavior results in the formation of large skyrmion bubbles (Figure 2c). The annihilation of these bubbles is accompanied by a contraction of 2π domain walls that separate the inside part of the bubble from the outside ferromagnetic medium (Figure 2d). These quasi-one-dimensional topological domain walls tend to collapse into small skyrmions with core magnetizations anti-aligned with both the applied field and the original skyrmion core magnetization (Figure 2e). Eventually, the domain walls vanish, and only a

low density of core-inverted skyrmions is observed for sufficiently negative magnetic fields (Figure 2f). The in-plane magnetization direction of the skyrmions in Figures 2a–f is given by the colors shown in Figures 2g,h. A magnified schematic showing the reversal of the skyrmion internal structure in more detail is shown in Figures 3a–h. Recent theoretical [51] and experimental [52] works have identified the large change in skyrmion size under positive magnetic field, and formation of the large patch-like structures for negative magnetic fields, as signatures of predominantly dipolar-stabilised spin textures in magnetic thin films and multilayers with the interfacial DMI. We note that in $\text{Co}_9\text{Zn}_9\text{Mn}_2$ the spiral pitch and the skyrmion size are independent from the sample dimensions, and show similar periodicities in bulk crystals and a few-hundred nanometer thick plates [19]. Therefore, while the dipolar interaction may impact the behaviour of the SkX under positive or negative magnetic fields, the ground state periodicity λ is determined by the dominant DM and exchange interactions.

For comparison, we applied the same protocol to determine the total topological charge and system energy for equilibrium SkX nucleation from a starting zero-field helical state. In this case, the magnetization evolves from a single-domain helix to helicoidal structure, and finally, to a SkX pattern upon increasing the field.

The field-dependence of the calculated topological charge for the processes of both SkX inversion and SkX nucleation from helical order are shown in Figure 4a. The field region $300 < |B| < 420$ mT over which the SkX inversion takes place is highlighted. The simulation results for SkX collapse are qualitatively consistent with the LTEM data: the gradual expansion of the metastable skyrmions takes place upon sweeping the field from 0 to ~ 290 mT, followed by inversion of the total topological charge Q from negative to positive. Experimentally, we find the magnitude of topological charge reversal to be 1% which is in good agreement with a reversed skyrmion fraction of 2.8% suggested by the simulation. Surprisingly, we find SkX nucleation from the helical phase requires a much higher negative magnetic field than that required for the inversion of metastable skyrmions (Figure 4a). A small hump in the magnetic field dependence of the total Q during the nucleation process at $|B| = 280 - 320$ mT (see Figure S1 in the Supplementary material [53]) is possibly due to the annihilation of meron defects and single helicoids followed by the creation of isolated skyrmions. At higher field, skyrmions emerge coherently from the rest of the helicoidal texture. The absolute values of the final topological charge in the SkX inversion and SkX nucleation scenarios are not the same due to the difference in the initial number of skyrmions in the starting condition (random spin orientation vs helical pattern). Figure 4b shows the magnetic field dependence of the total system energy. In the whole field range from zero to $|B| \approx 300$ mT the helical (helicoidal) state is

energetically favorable, thus emphasizing the metastable character of the starting SkX considered for the SkX collapse process. Crucially, we find the system achieves an energy gain through the stabilization of skyrmions with inverted core magnetizations. This underlines the energetic advantage of the direct skyrmion inversion scenario compared to a SkX to helicoid transition under the application of negative magnetic fields. Interestingly, this energy gain is not reproduced in a simulation with of a sample of smaller dimension (see Supplementary material [53]) due to finite-size effects and the formation of skyrmion bags in this case. A similar phenomena was observed in a 150 nm-thick FeGe thin plate at low temperature, when field-cooled metastable skyrmions were packed into a bundle by a field cycling procedure [54].

Overall, our experimental results are consistent with a field-driven, second-order "topological melting" transition of the metastable SkX in the presence of defects described in Ref. 40. In contrast to the "topological switching" phenomena mediated by anti-skyrmions, the melting scenario does not include the conservation of the total topological charge in the system $|Q| = |n| \cdot N_{sk}$, where n is the topological number as defined in the Equation 1, and N_{sk} is the number of skyrmions in the sample. As the total number of skyrmions N_{sk} is reduced in the melting process to $\sim 1\%$ of its original value, only partial topological charge inversion takes place (Figure 4a). The described process of the SkX inversion is qualitatively similar to the classical process of magnetic bubble domain array reversal in PMA systems without DMI, also known as "topological melting" [37–39].

In Ref. 40 the presence of defects was found essential to induce skyrmion melting process, where the defect site acts as a "topological-charge sink". Note, that our simulations did not imply any artificially introduced defects, such as randomly distributed non-magnetic sites or regions with pinned magnetization or anisotropy axes. Instead, the distorted SkX as seen in Figure 3a is formed by the relaxation of random magnetization pattern in an applied field (see Supplementary materials for simulation details). The packing defects of this lattice are similar to the ones observed in the experimental data (Figure 1)b and assist the "topological melting" scenario.

III. CONCLUSIONS

Taken together, our LTEM experiments and micro-magnetic simulations clearly demonstrate for the first time a successful inversion of the topological charge in a thin plate of a chiral magnet. The negative field-driven transformation of the SkX is conceivably due to the enhanced energetic stability (so-called topological protection) of zero-field skyrmions at room temperature compared with the thermodynamically stable helical phase. This scenario contrasts strongly with the direct skyrmion-to-helical conversion reported for metastable skyrmions in FeGe and $\text{Fe}_{0.5}\text{Co}_{0.5}\text{Si}$ [26, 43, 55]. Our

micromagnetic simulations of both the skyrmion inversion and skyrmion nucleation processes qualitatively explain our results from the point of view of the energetics. The time resolution of present LTEM observation was not sufficient to describe this process dynamically and identify anti-skyrmion creation that possibly accompanies the skyrmion merging process [14, 40]. This issue should be further addressed by ultrafast pump-probe LTEM and x-ray imaging studies [56–58]. Finally, we have shown that the negative field-driven merging of metastable skyrmions leads to the formation of large skyrmion bubbles separated by 2π domain walls. The realization of such large skyrmion bubbles in $\text{Co}_9\text{Zn}_9\text{Mn}_2$ is furthermore a promising step towards the engineering of novel chiral magnetic particles with any integer topological charge ("skyrmion bags" and "skyrmion bundles") considered in the theory of Refs. [59, 60], and recently realized experimentally in FeGe [54]. In this instance, it is expected that smaller skyrmions can be nucleated inside the large bubbles by electric current [61], optical and x-ray light pulses [56, 62, 63] or a scanning tunneling microscope tip [64], thus providing new and novel means for topological charge modulation and control.

IV. EXPERIMENTAL SECTION

Samples

The details of sample preparation and the structure of the magnetic phase diagrams in both bulk and thin plate samples are given in Ref. 20.

Real-space imaging

The real-space imaging of the negative magnetic field-driven collapse of the metastable SkX in a ~ 150 nm-thick $\text{Co}_9\text{Zn}_9\text{Mn}_2$ plate was carried out by means of Lorentz transmission electron microscopy (LTEM). Measurements were performed with a transmission electron microscope (JEM-2100F) at an acceleration voltage of 200 kV, and the defocus distances of $\pm 288 \mu\text{m}$ as described in the main text.

SUPPLEMENTARY INFORMATION

Supporting Information is available from the Wiley Online Library at the link [53] or from the author.

ACKNOWLEDGEMENTS

This research was supported in part by JSPS Grant-in-Aids for Scientific Research (Grant No. 20K15164). V.U. and J.S.W. acknowledge funding from the SNSF Sinergia CRSII5_171003 NanoSkyrmionics.

-
- [1] A. Bogdanov and A. Hubert, Thermodynamically stable magnetic vortex states in magnetic crystals, *Journal of Magnetism and Magnetic Materials* **138**, 255 (1994).
 - [2] N. Nagaosa and Y. Tokura, Topological properties and dynamics of magnetic skyrmions, *Nature Nanotechnology* **8**, 899 (2013).
 - [3] S. Mühlbauer, B. Binz, F. Jonietz, C. Pfleiderer, A. Rosch, A. Neubauer, R. Georgii, and P. Böni, Skyrmion lattice in a chiral magnet, *Science* **323**, 915 (2009).
 - [4] XZ. Yu, N. Kanazawa, Y. Onose, K. Kimoto, W. Zhang, S. Ishiwata, Y. Matsui, and Y. Tokura, Near room-temperature formation of a skyrmion crystal in thin-films of the helimagnet fege, *Nature Materials* **10**, 106 (2011).
 - [5] S. Seki, XZ. Yu, S. Ishiwata, and Y. Tokura, Observation of skyrmions in a multiferroic material, *Science* **336**, 198 (2012).
 - [6] Y. Tokunaga, XZ. Yu, J. White, H. M. Rønnow, D. Morikawa, Y. Taguchi, and Y. Tokura, A new class of chiral materials hosting magnetic skyrmions beyond room temperature, *Nature Communications* **6**, 7638 (2015).
 - [7] I. Kézsmárki, S. Bordács, P. Milde, E. Neuber, L. Eng, J. White, H. M. Rønnow, C. Dewhurst, M. Mochizuki, K. Yanai, *et al.*, Néel-type skyrmion lattice with confined orientation in the polar magnetic semiconductor GaV_4S_8 , *Nature Materials* **14**, 1116 (2015).
 - [8] T. Kurumaji, T. Nakajima, V. Ukleev, A. Feoktystov, T.-h. Arima, K. Kakurai, and Y. Tokura, Néel-type skyrmion lattice in the tetragonal polar magnet V_2O_5 , *Physical Review Letters* **119**, 237201 (2017).
 - [9] XZ. Yu, Y. Tokunaga, Y. Kaneko, W. Zhang, K. Kimoto, Y. Matsui, Y. Taguchi, and Y. Tokura, Biskyrmion states and their current-driven motion in a layered manganite, *Nature Communications* **5**, 3198 (2014).
 - [10] J. T. Lee, J. Chess, S. Montoya, X. Shi, N. Tamura, S. Mishra, P. Fischer, B. McMorrán, S. Sinha, E. Fullerton, *et al.*, Synthesizing skyrmion bound pairs in Fe-Gd thin films, *Applied Physics Letters* **109**, 022402 (2016).
 - [11] W. Wang, Y. Zhang, G. Xu, L. Peng, B. Ding, Y. Wang, Z. Hou, X. Zhang, X. Li, E. Liu, *et al.*, A centrosymmetric hexagonal magnet with superstable biskyrmion magnetic nanodomains in a wide temperature range of 100–340 K, *Advanced Materials* **28**, 6887 (2016).

- [12] R. Takagi, XZ. Yu, J. White, K. Shibata, Y. Kaneko, G. Tatara, H. Rønnow, Y. Tokura, and S. Seki, Low-field bi-skyrmion formation in a noncentrosymmetric chimney ladder ferromagnet, *Physical Review Letters* **120**, 037203 (2018).
- [13] A. K. Nayak, V. Kumar, T. Ma, P. Werner, E. Pippel, R. Sahoo, F. Damay, U. K. Rößler, C. Felser, and S. S. Parkin, Magnetic antiskyrmions above room temperature in tetragonal heusler materials, *Nature* **548**, 561 (2017).
- [14] W. Koshibae and N. Nagaosa, Theory of antiskyrmions in magnets, *Nature Communications* **7**, 10542 (2016).
- [15] A. Fert, N. Reyren, and V. Cros, Magnetic skyrmions: advances in physics and potential applications, *Nature Reviews Materials* **2**, 17031 (2017).
- [16] T. Adams, A. Chacon, M. Wagner, A. Bauer, G. Brandl, B. Pedersen, H. Berger, P. Lemmens, and C. Pfleiderer, Long-wavelength helimagnetic order and skyrmion lattice phase in Cu_2OSeO_3 , *Physical Review Letters* **108**, 237204 (2012).
- [17] W. Münzer, A. Neubauer, T. Adams, S. Mühlbauer, C. Franz, F. Jonietz, R. Georgii, P. Böni, B. Pedersen, M. Schmidt, *et al.*, Skyrmion lattice in the doped semiconductor $\text{Fe}_{1-x}\text{Co}_x\text{Si}$, *Physical Review B* **81**, 041203 (2010).
- [18] N. Kanazawa, J.-H. Kim, D. Inosov, J. White, N. Egetenmeyer, J. Gavilano, S. Ishiwata, Y. Onose, T.-h. Arima, B. Keimer, *et al.*, Possible skyrmion-lattice ground state in the b20 chiral-lattice magnet MnSi as seen via small-angle neutron scattering, *Physical Review B* **86**, 134425 (2012).
- [19] K. Karube, J. White, N. Reynolds, J. Gavilano, H. Oike, A. Kikkawa, F. Kagawa, Y. Tokunaga, H. M. Rønnow, Y. Tokura, *et al.*, Robust metastable skyrmions and their triangular-square lattice structural transition in a high-temperature chiral magnet, *Nature Materials* **15**, 1237 (2016).
- [20] K. Karube, J. White, D. Morikawa, M. Bartkowiak, A. Kikkawa, Y. Tokunaga, T.-h. Arima, H. Rønnow, Y. Tokura, and Y. Taguchi, Skyrmion formation in a bulk chiral magnet at zero magnetic field and above room temperature, *Physical Review Materials* **1**, 074405 (2017).
- [21] D. Morikawa, XZ. Yu, K. Karube, Y. Tokunaga, Y. Taguchi, T.-h. Arima, and Y. Tokura, Deformation of topologically-protected supercooled skyrmions in a thin plate of chiral magnet $\text{Co}_8\text{Zn}_8\text{Mn}_4$, *Nano Letters* **17**, 1637 (2017).
- [22] K. Karube, J. S. White, D. Morikawa, C. D. Dewhurst, R. Cubitt, A. Kikkawa, XZ. Yu, Y. Tokunaga, T.-h. Arima, H. M. Rønnow, *et al.*, Disordered skyrmion phase stabilized by magnetic frustration in a chiral magnet, *Science Advances* **4**, eaar7043 (2018).
- [23] V. Ukleev, Y. Yamasaki, D. Morikawa, K. Karube, K. Shibata, Y. Tokunaga, Y. Okamura, K. Amemiya, M. Valvidares, H. Nakao, *et al.*, Element-specific soft x-ray spectroscopy, scattering, and imaging studies of the skyrmion-hosting compound $\text{Co}_8\text{Zn}_8\text{Mn}_4$, *Physical Review B* **99**, 144408 (2019).
- [24] T. Nagase, Y.-G. So, H. Yasui, T. Ishida, H. K. Yoshida, Y. Tanaka, K. Saitoh, N. Ikarashi, Y. Kawaguchi, M. Kuwahara, *et al.*, Observation of domain wall bimerons in chiral magnets, *Nature Communications* **12**, 1 (2021).
- [25] P. Bak and M. H. Jensen, Theory of helical magnetic structures and phase transitions in MnSi and FeGe , *Journal of Physics C: Solid State Physics* **13**, L881 (1980).
- [26] A. Kovács, Z.-A. Li, K. Shibata, and R. E. Dunin-Borkowski, Lorentz microscopy and off-axis electron holography of magnetic skyrmions in FeGe , *Resolution and Discovery* **1**, 2 (2016).
- [27] A. Thiele, The theory of cylindrical magnetic domains, *The Bell System Technical Journal* **48**, 3287 (1969).
- [28] A. Malozemoff and K. Papworth, High-speed photography of topological switching and anisotropic saturation velocities in a misoriented garnet film, *Journal of Physics D: Applied Physics* **8**, 1149 (1975).
- [29] A. B. Bogatyrev and K. L. Metlov, What makes magnetic skyrmions different from magnetic bubbles?, *Journal of Magnetism and Magnetic Materials* **465**, 743 (2018).
- [30] XZ. Yu, Y. Tokunaga, Y. Taguchi, and Y. Tokura, Variation of topology in magnetic bubbles in a colossal magnetoresistive manganite, *Advanced Materials* **29**, 1603958 (2017).
- [31] J. C. Loudon, A. C. Twitchett-Harrison, D. Cortés-Ortuño, M. T. Birch, L. A. Turnbull, A. Štefančič, F. Y. Ogrin, E. O. Burgos-Parra, N. Bukin, A. Laurenson, *et al.*, Do images of biskyrmions show type-II bubbles?, *Advanced Materials* **31**, 1806598 (2019).
- [32] S. Grigoriev, D. Chernyshov, V. Dyadkin, V. Dmitriev, S. Maleyev, E. Moskvina, D. Menzel, J. Schoenes, and H. Eckerlebe, Crystal handedness and spin helix chirality in $\text{Fe}_{1-x}\text{Co}_x\text{Si}$, *Physical Review Letters* **102**, 037204 (2009).
- [33] D. Morikawa, K. Shibata, N. Kanazawa, XZ. Yu, and Y. Tokura, Crystal chirality and skyrmion helicity in MnSi and $(\text{Fe},\text{Co})\text{Si}$ as determined by transmission electron microscopy, *Physical Review B* **88**, 024408 (2013).
- [34] T. O'Dell, The dynamics of magnetic bubble domain arrays, *Philosophical Magazine* **27**, 595 (1973).
- [35] K. Papworth, The topological switching of magnetic bubble domain arrays, *IEEE Transactions on Magnetics* **10**, 638 (1974).
- [36] V. Randoshkin, L. Ivanov, and R. Telesnin, „dynamics of domains in iron garnet films in a homogeneous magnetic field”, *Sov. Phys. JETP* **48**, 486 (1978).
- [37] K. Babcock and R. Westervelt, Topological “melting” of cellular domain lattices in magnetic garnet films, *Physical Review Letters* **63**, 175 (1989).
- [38] V. Zablotskii and Y. A. Mamalui, Ordering and “melting” of domain lattices in thin magnetic films, *Journal of Physics: Condensed Matter* **7**, 5271 (1995).
- [39] E. A. Jagla, Numerical simulations of two-dimensional magnetic domain patterns, *Physical Review E* **70**, 046204 (2004).
- [40] L. Pierobon, C. Moutafis, Y. Li, J. Löffler, and M. Charilaou, Collective antiskyrmion-mediated phase transition and defect-induced melting in chiral magnetic films., *Scientific Reports* **8**, 16675 (2018).
- [41] C. Heo, N. S. Kiselev, A. K. Nandy, S. Blügel, and T. Rasing, Switching of chiral magnetic skyrmions by picosecond magnetic field pulses via transient topological states, *Scientific Reports* **6**, 27146 (2016).
- [42] J. Wild, T. N. Meier, S. Pöllath, M. Kronseder, A. Bauer, A. Chacon, M. Halder, M. Schowalter, A. Rosenauer, J. Zweck, *et al.*, Entropy-limited topological protection of skyrmions, *Science Advances* **3**, e1701704 (2017).
- [43] L. Peng, Y. Zhang, L. Ke, T.-H. Kim, Q. Zheng, J. Yan, X.-G. Zhang, Y. Gao, S. Wang, J. Cai, *et al.*, Relaxation dynamics of zero-field skyrmions over a wide temperature

- range, Nano Letters **18**, 7777 (2018).
- [44] XZ. Yu, W. Koshibae, Y. Tokunaga, K. Shibata, Y. Taguchi, N. Nagaosa, and Y. Tokura, Transformation between meron and skyrmion topological spin textures in a chiral magnet, Nature **564**, 95 (2018).
 - [45] D. McGrouther, R. Lamb, M. Krajnak, S. McFadzean, S. McVitie, R. Stamps, A. Leonov, A. Bogdanov, and Y. Togawa, Internal structure of hexagonal skyrmion lattices in cubic helimagnets, New Journal of Physics **18**, 095004 (2016).
 - [46] XZ. Yu, D. Morikawa, T. Yokouchi, K. Shibata, N. Kanazawa, F. Kagawa, T.-h. Arima, and Y. Tokura, Aggregation and collapse dynamics of skyrmions in a non-equilibrium state, Nature Physics **14**, 832 (2018).
 - [47] N. Romming, A. Kubetzka, C. Hanneken, K. von Bergmann, and R. Wiesendanger, Field-dependent size and shape of single magnetic skyrmions, Physical Review Letters **114**, 177203 (2015).
 - [48] A. Vansteenkiste, J. Leliaert, M. Dvornik, M. Helsen, F. Garcia-Sanchez, and B. Van Waeyenberge, The design and verification of mumax3, AIP Advances **4**, 107133 (2014).
 - [49] R. Takagi, D. Morikawa, K. Karube, N. Kanazawa, K. Shibata, G. Tatara, Y. Tokunaga, T.-h. Arima, Y. Taguchi, Y. Tokura, *et al.*, Spin-wave spectroscopy of the dzyaloshinskii-moriya interaction in room-temperature chiral magnets hosting skyrmions, Physical Review B **95**, 220406 (2017).
 - [50] B. Berg and M. Lüscher, Definition and statistical distributions of a topological number in the lattice $\phi(3)$ -model, Nuclear Physics B **190**, 412 (1981).
 - [51] F. Büttner, I. Lemesch, and G. S. Beach, Theory of isolated magnetic skyrmions: From fundamentals to room temperature applications, Scientific Reports **8**, 1 (2018).
 - [52] M. Birch, L. Powalla, S. Wintz, O. Hovorka, K. Litzius, J. Loudon, L. Turnbull, V. Nehruji, K. Son, C. Bubeck, *et al.*, History-dependent domain and skyrmion formation in 2d van der waals magnet fe₃gete₂, Nature Communications **13**, 1 (2022).
 - [53] See Supplemental Material at <https://...> for more details on micromagnetic simulation. (2022).
 - [54] J. Tang, Y. Wu, W. Wang, L. Kong, B. Lv, W. Wei, J. Zang, M. Tian, and H. Du, Magnetic skyrmion bundles and their current-driven dynamics, Nature Nanotechnology **16**, 1086 (2021).
 - [55] P. Milde, D. Köhler, J. Seidel, L. Eng, A. Bauer, A. Chacon, J. Kindervater, S. Mühlbauer, C. Pfleiderer, S. Buhardt, *et al.*, Unwinding of a skyrmion lattice by magnetic monopoles, Science **340**, 1076 (2013).
 - [56] G. Berruto, I. Madan, Y. Murooka, G. Vanacore, E. Pomarico, J. Rajeswari, R. Lamb, P. Huang, A. Kruchkov, Y. Togawa, *et al.*, Laser-induced skyrmion writing and erasing in an ultrafast cryo-lorentz transmission electron microscope, Physical Review Letters **120**, 117201 (2018).
 - [57] F. Büttner, C. Moutafis, M. Schneider, B. Krüger, C. Günther, J. Geilhufe, C. v. K. Schmising, J. Mohanty, B. Pfau, S. Schaffert, *et al.*, Dynamics and inertia of skyrmionic spin structures, Nature Physics **11**, 225 (2015).
 - [58] K. Litzius, I. Lemesch, B. Krüger, P. Bassirian, L. Caretta, K. Richter, F. Büttner, K. Sato, O. A. Tretiakov, J. Förster, *et al.*, Skyrmion hall effect revealed by direct time-resolved x-ray microscopy, Nature Physics **13**, 170 (2017).
 - [59] F. N. Rybakov and N. S. Kiselev, Chiral magnetic skyrmions with arbitrary topological charge, Physical Review B **99**, 064437 (2019).
 - [60] D. Foster, C. Kind, P. J. Ackerman, J.-S. B. Tai, M. R. Dennis, and I. I. Smalyukh, Two-dimensional skyrmion bags in liquid crystals and ferromagnets, Nature Physics **15**, 1 (2019).
 - [61] XZ. Yu, D. Morikawa, Y. Tokunaga, M. Kubota, T. Kurumaji, H. Oike, M. Nakamura, F. Kagawa, Y. Taguchi, T.-h. Arima, *et al.*, Current-induced nucleation and annihilation of magnetic skyrmions at room temperature in a chiral magnet, Advanced Materials **29**, 1606178 (2017).
 - [62] S.-G. Je, P. Vallobra, T. Srivastava, J.-C. Rojas-Sánchez, T. H. Pham, M. Hehn, G. Malinowski, C. Baraduc, S. Auffret, G. Gaudin, *et al.*, Creation of magnetic skyrmion bubble lattices by ultrafast laser in ultrathin films, Nano Letters **18**, 7362 (2018).
 - [63] Y. Guang, I. Bykova, Y. Liu, G. Yu, E. Goering, M. Weigand, J. Gräfe, S. K. Kim, J. Zhang, H. Zhang, *et al.*, Creating zero-field skyrmions in exchange-biased multilayers through x-ray illumination, Nature Communications **11**, 1 (2020).
 - [64] R. Wieser, R. Shindou, and X. Xie, Manipulation of magnetic skyrmions with a scanning tunneling microscope, Physical Review B **95**, 064417 (2017).